Path planning under localization uncertainty

Yang Gao[1,2,*], Hao Xu[1], Mengqi Hu[2], Jiang Liu[1], Jiahao Liu[1]

1. School of Automobile, Chang'An University, Xi'an 710064, China

*2. Department of Mechanical and Industrial Engineering,
University of Illinois at Chicago, Chicago, Illinois, USA*

nchygy@126.com

ABSTRACT. This paper attempts to disclose the impact of localization uncertainty on path planning, a key function of mobile robot. Firstly, the localization uncertainty was analyzed in details, revealing that the uncertainty can be represented by the half length of the possible distribution area of the X-Y coordinates or the orientation variance. After that, the impact of uncertainty on path planning was evaluated in light of the path planning safety and performance. Then, two evaluation functions were put forward to evaluate the impact of uncertainty on path planning. Through simulation and experiment, the proposed functions were proved feasible and valid. The research findings shed new light on path planning under localization uncertainty.

RÉSUMÉ. Cet article tente de révéler l'impact de l'incertitude de localisation sur la planification de chemin, une fonction clé du robot mobile. Premièrement, l'incertitude de localisation a été analysée en détail, révélant que l'incertitude peut être représentée par la demi-longueur de l'aire de répartition possible des coordonnées X-Y ou la variance d'orientation. Après cela, l'impact de l'incertitude sur la planification du chemin a été évalué à la lumière de la sécurité et de la performance de la planification du chemin. Ensuite, deux fonctions d'évaluation ont été proposées pour évaluer l'impact de l'incertitude sur la planification du chemin. Par la simulation et l'expérimentation, les fonctions proposées se sont avérées réalisables et valides. Les résultats de la recherche ont jeté un nouvel éclairage sur la planification de la trajectoire dans des conditions de localisation incertaine.

KEYWORDS: Path planning, localization, map matching, mobile robot.

MOTS-CLÉS: chemin suivi, planification de chemin, localisation, correspondance de carte, robot mobile.

1. Introduction

Mobile robots generally rely on the localization results to follow the planned path. Uncertainty in localization may negatively affect the path planning and path following. However, there is little report on the impact of localization uncertainty on path planning.

The existing studies often describe localization uncertainty by the distribution covariance of locations and treat it the same as localizability. Roy *et al.* (1999) were the first to study the uncertainty in localization and localizability. Li and Franck measured the confidence of the information from the positioning system using map-aided horizontal uncertainty level meter. References (Yang *et al.*, 2015) explore the localization uncertainty and localizability in wireless network localization.

The localization uncertainty and localizability have been extensively investigated in the map-based localization methods, in which the robot localizes itself by matching its perception with the given map through dead-reckoning (Qian *et al.*, 2016). Assuming that the map is binary and the obstacle is differentiable, Censi (2007) determined the theoretical precision limit of map-based localization methods based on Cramér–Rao bound, defined localizability as the low bound of the localization uncertainty of the robot, and proposed a series of localizability estimation methods. Qian *et al.* (2016) introduced the influence factor of dynamic obstacles to estimate the localizability. Wang *et al.* (2015) developed a localizability-based action selection mechanism for mobile robots to speed up the convergence of global localization, in which the possible observation distinctness after a given action is predicted by a utility function. Ruiz-Mayor *et al.* proposed a new approach to estimate the perceptual ambiguity associated with localization uncertainty, and created a new probabilistic model of indistinguishability for perception with different kinds of range sensors (Murtra *et al.*, 2008).

The localization uncertainty has been taken into account in many recent studies on path or motion planning. For instance, Gonzalez and Stentz (2007) pursued the lowest expected cost, taking the localization uncertainty as a threat to the target reachability. Hu *et al.* (2012) presented a path planning algorithm for a mobile manipulator based on localizability, evaluated the localizability of a given path by adding up the fisher matrix along the path, and selected the path with the best localizability. Considering the localization uncertainty of the path, Robert *et al.* put forward a path planning algorithm after evaluating the uncertainties along the path and taking the localization uncertainty as a negative issue.

To sum up, the previous research has shown that the localization uncertainty has a negative impact to path or motion planning. However, more analysis is needed to identify and evaluate the exact impact. Hence, this paper attempts to disclose the impact of uncertain localization on path planning and develop evaluation functions for the impact (Zhao *et al.*, 2000).

The remainder of this paper is organized as follows: Section 2 discusses the impact of localization uncertainty on path planning and path following; Section 3 puts forward the evaluation functions for this impact; Section 4 verifies the performance

of the functions through evaluation; Section 5 further validates the functions through an experiment in a close environment; Section 6 wraps up this paper with several conclusions.

2. Impact of localization uncertainty on path planning

Let $S(x, y, \theta)$ be the position of the robot. The estimated position $\hat{S}$ obeys the Gaussian distribution $\hat{S} \sim N(S, \hat{\delta}_S)$, where $\hat{\delta}_S$ is the covariance matrix of the uncertainty of $\hat{\delta}_S$. If the covariance of the estimated X-Y coordinates of the robot is denoted as $\hat{\delta}_{XY}$, then $\hat{\delta}_S$ can be expressed as $(\hat{\delta}_{XY}, \hat{\delta}_\theta)$ by ignoring the covariance between the estimated θ and the X-Y coordinates. It can be found that $\hat{\delta}_S$ defines an ellipsoid shape probability distribution of $\hat{S}$, and $\hat{\delta}_{XY}$ defines the projection of $\hat{\delta}_S$ onto the plane of X-Y coordinates, which obeys an ellipse shape probability distribution.

The impact of localization uncertainty under the above assumptions is illustrated in Figure 1, where the triangles are the robot poses, the dashed ellipses are defined by the $\hat{\delta}_{XY}$, and the solid line is the given path. To tolerate motion and localization errors, all obstacles are generally inflated by a safe radius r_s, and the destination by another safe radius r_a. In Figure 1, the obstacles are in black, the destination is in red and the inflated regions are circled by dash lines. The localization uncertainty directly affects path following before acting on path planning. Thus, the impact of localization uncertainty on path planning is here converted into that on path following. The blue point in Figure 1 stands for the following target, which is generally employed in path following algorithms (Egerstedt *et al.*, 2001).
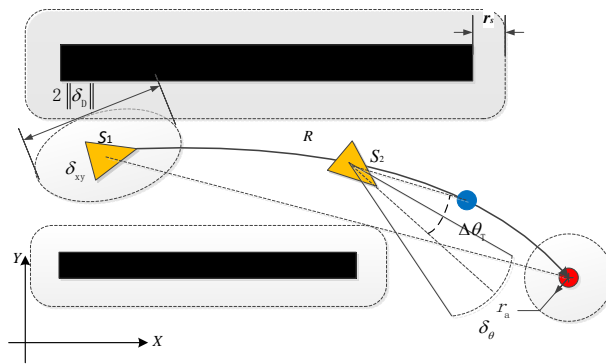

Figure 1. The impact of localization uncertainty on path following

2.1. The impact of $\widehat{\delta}_\theta$

Generally, the robot moves to reduce the angle difference $\Delta\theta_T$ between its orientation and the direction of the following target. Thus, the motion control of robot orientation can be simplified as:

$$\theta_k = \theta_{k-1} - \gamma \Delta\theta_T \tag{1}$$

where k is the value at time k; γ is a variable related to control policy. Without considering the limited turning ability of the robot, the value of γ was set to 1.

Let $\hat{\theta}_k$ be the estimated θ_k which conforms to the Gaussian distribution ($\hat{\theta}_k \sim N(\theta_k, \delta_\theta)$). Then, the current post $\hat{S}_k$ can be estimated from the robot motion model:

$$
\begin{aligned}
\hat{x}_k &= \hat{x}_{k-1} + v\Delta t \cos(\hat{\theta}_k) \\
\hat{y}_k &= \hat{y}_{k-1} + v\Delta t \sin(\hat{\theta}_k) \\
\hat{\theta}_k &= \hat{\theta}_{k-1} + \hat{\delta}_{\theta k-1} - \Delta\theta_T
\end{aligned}
\tag{2}
$$

where v is the translational speed of the robot; Δt is the time span between two time steps. According to the knowledge of variance, we have $\theta_{k-1} - \hat{\delta}_{\theta k-1} \leq \hat{\theta}_{k-1} \leq \theta_{k-1} + \hat{\delta}_{\theta k-1}$ with the probability of about 0.683. Since the limited turning ability of the robot is not taken into account, the robot can always turn to the desired orientation in one time step and the estimation error of $\hat{\theta}_{k-1}$ always reaches $\hat{\delta}_{\theta k-1}$. Then, equation (1) can be rewritten as:

$$\hat{\theta}_k = \theta_{k-1} + \hat{\delta}_{\theta k-1} - \Delta\theta_T \tag{3}$$

Assuming that the start point is $S_0(X_0,0,0)$, $X_0=50$ and $r_a=5$, the path of the robot can be plotted from S_0 to the destination with a fix estimation error $\hat{\delta}_\theta$ in accordance with equations (2) and (3). Figure 2 presents the paths obtained by different $\hat{\delta}_\theta$ values, in which the cross is the start point, the red dot is the destination and the red dashed line is the r_a. It can be seen that the path became longer as $\hat{\delta}_\theta$ increased from 0.3 to 1.97, and that the robot could never each the destination if $\hat{\delta}_\theta \geq \frac{\pi}{2}$. Figure 3 illustrates the exponentially increasing relationship between $\hat{\delta}_\theta$ and the path length L(cm).
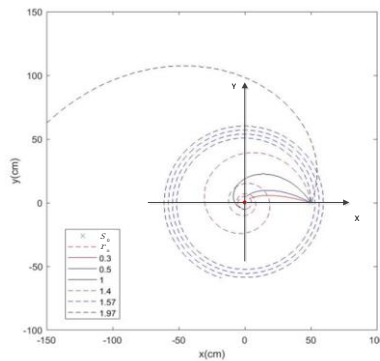

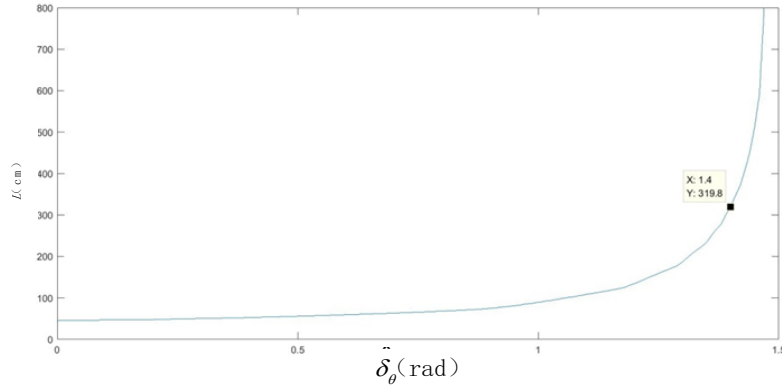Figure 2. The robot paths obtained at different $\hat{\delta}_\theta$ values

Figure 3. The relationship between $\hat{\delta}_\theta$ and L

Figure 4 shows the relationship between $\hat{\delta}_\theta$ and L under different start points X_0=(50cm, 100cm, 200cm), where the value of X_0 refers to the distance between the start point and the destination. It can be seen that the relationship differed greatly with the distances. However, if the L is replaced by $\frac{L}{X_0}$, then the relationships in Figure 4 can be converted to the three solid lines in Figure 5, where the green, red and black solid lines represent the relationships under different values of X_0.
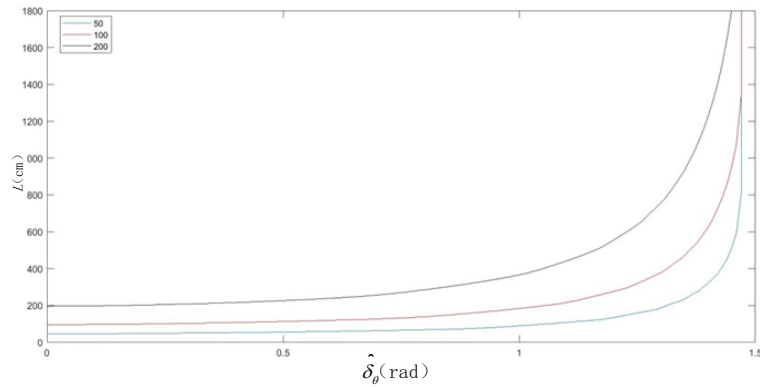

Figure 4. The relationship between $\hat{\delta}_\theta$ and L at different X_0 values

Next, the relationships in Figure 5 were fitted in the Matlab, yielding a unified relationship with a RMSE 0.07373. Thus, the impact of $\hat{\delta}_\theta$ on path following can be described as:

$$\frac{L}{X_0} = \frac{X_0(\frac{p_1}{\delta_\theta} + p_2)}{\left(\delta_\theta^2 + q_1\delta_\theta + q_2\right)} \qquad (4)$$

where p_1=-6,375; p_2=3.766e+04; q_1=-1.436e+04; q_2=2.669e+04.
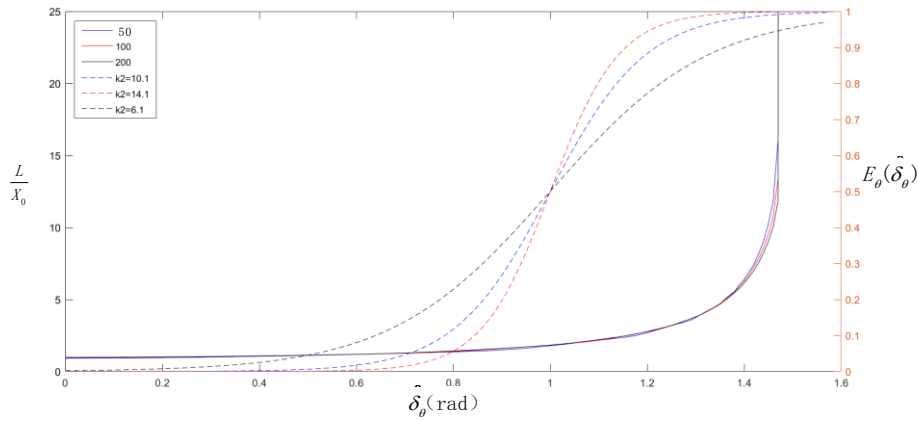

Figure 5. The relationship between $\frac{L}{X_0}$ and $\hat{\delta}_\theta$ at different X_0 values and that between $E_\theta(\hat{\delta}_\theta)$ and $\hat{\delta}_\theta$ at different k_2 values

2.2. The impact of $\widehat{\delta}_{XY}$

The X-Y coordinates of the robot are most likely to fall in the ellipse region of $\hat{\delta}_{XY}$. Let $\|\hat{\delta}_D\|$ be the half length of the longer axis of the ellipse of $\hat{\delta}_{XY}$. According to the knowledge about bivariate normal distribution, it is easy to learn that $\|\hat{\delta}_D\|$ can be derived from equation (5) if $1-\alpha$ is the probability that the robot is located within the ellipse whose longer axis is $\|\hat{\delta}_D\|$ in length.

$$\left\|\hat{\delta}_D\right\| = \sqrt{\chi^2_2(\alpha)\lambda_{max}} \qquad (5)$$

Let $x_2^2(\alpha)$ denote the upper (100α)-th percentile of a 2DOF x^2 distribution and λ_{max} denote the maximum eigenvalue of δ_{XY}. Then, $\hat{\delta}_{XY}$ can be safely represented by $\|\hat{\delta}_D\|$, indicating that the probability that the robot position lies in the circle with a radius of $\|\hat{\delta}_D\|$ is no less than $1 - \alpha$. For simplicity, it is assumed that $x_2^2(\alpha) = 1$. Then, δ_s can be described by $(\|\hat{\delta}_D\|, \hat{\delta}_\theta)$.

In path planning, the optimal path is generally close to the edge of the obstacles to reduce the total length. Thus, if a position has a large $\|\hat{\delta}_D\|$, that is, a large area of probability distribution, then path traversing this position is highly likely to collide

into obstacles. In other words, the larger the $\|\hat{\delta}_D\|$ of the pose, the worse the path traversing the pose. To reduce the possibility of collision, $\|\hat{\delta}_D\|$ should satisfy the following condition:

$$r_s > \left\|\delta_D\right\| + r_R \tag{6}$$

where r_R is the safe radius of the robot. Equation (6) means the localization error should fall within the tolerance range defined by r_R and r_s. To reduce the risk that the robot cannot reach the destination due to localization error, the position estimation error should satisfy the following condition:

$$\left\|\delta_D\right\| < r_a \tag{7}$$

where r_a is the given tolerance range.

3. Evaluation functions for the impact of localization uncertainty

3.1. Evaluation function for the impact of $\hat{\delta}_\theta$

In path planning, an evaluation function is required to map the negative impact to a limited value domain. Some path planning approaches prefer to use a differentiable evaluation function. In light of the previous analysis, a sigmoid function was adopted to evaluate the impacts of $\|\hat{\delta}_D\|$ and $\hat{\delta}_\theta$ separately.

Considering the negative impact of $\hat{\delta}_\theta$ on the path, the evaluation fuction $E_\theta(\hat{\delta}_\theta)$ was constructed as:

$$E_\theta(\hat{\delta}_\theta) = sig(\hat{\delta}_\theta) = \frac{1}{1+e^{-k_2(\delta_\theta - \frac{\theta_{u2}}{2})}} \tag{8}$$

where θ_{u2} is a manually adjusted parameter, which comes from the fact that the robot cannot reach the destination if $\delta_\theta \geq \frac{\pi}{2}$ and $E_\theta\left(\frac{\theta_{u2}}{2}\right) = 0.5$; k_2 is the increasing rate of the evaluation value. k_2 is also manually adjusted parameter. The evaluation value of $E_\theta(\hat{\delta}_\theta)$ is negatively correlated with the impact of $\hat{\delta}_\theta$.

In Figure 5, the dashed curves depict the relationships between $E_\theta(\hat{\delta}_\theta)$ and $\hat{\delta}_\theta$. Focusing on the right vertical axis, with $\theta_{u2}=2$, k_2 can be set to 6.1, 10.1 and 14.1, respectively. Here, the parameter values are configured as $k_2=14.1$ and $\theta_{u2}=2$. In this case, $E_\theta(1) = 0.5$ and $E_\theta(1.4) \approx 1$.

3.2. Evaluation function for the impact of $||\hat{\delta}_D||$

The impact of $||\hat{\delta}_D||$ can be evaluated by the following evaluation function $E(||\hat{\delta}_D||)$:

$$E\left(\left\|\hat{\delta}_D\right\|\right) = sig\left(\left\|\hat{\delta}_D\right\|\right) = \frac{1}{1+e^{-k_1\left(\left\|\hat{\delta}_D\right\|-\frac{r_u}{2}\right)}} \tag{9}$$

where r_u is the lowest bound; k_1 is the increase rate of the evaluation value. The value of $E(||\hat{\delta}_D||)$ is negatively correlated with the impact of $||\hat{\delta}_D||$. The lowest bound can be obtained from equations (6) and (7):

$$r_u = \min(r_s - r_R, r_a) \tag{10}$$

Figure 6 shows six curves on the relationship between $||\hat{\delta}_D||$ and $E(||\hat{\delta}_D||)$ at k_1=0.2, 0.6, 1, 2, 3 and 4, respectively. In our research, the value of k_1 was set to 1 such that $E(r_u) \approx 1$ and the value of r_s, r_R and r_a were set to 50cm, 30cm and 50cm, respectively.
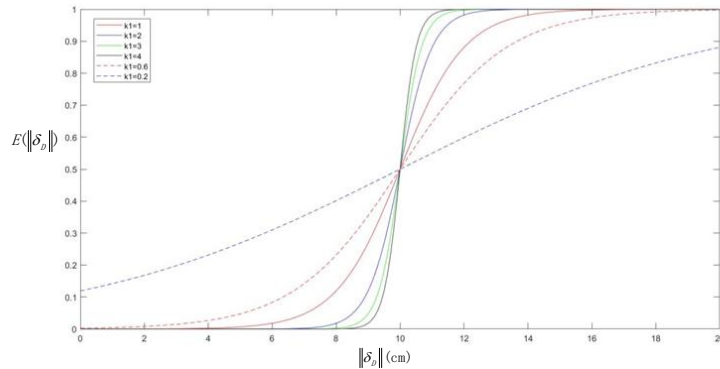

Figure 6. E($||\hat{\delta}_D||$) at different values of k1 and $||\hat{\delta}_D||$

4. Simulation verification

To prove the effect of the proposed approach, a simulation was carried out on Matlab in a typical indoor environment (Figure 7). During the simulation, a TurtleBot robot was required to move from the current position S_0 to the start point S_1 and then to the destination S_5 following a given path. The localization results were provided by augmented Monte-Carlo localization (AMCL). The virtual vehicle approach was employed to control the robot in this simulation and the subsequent experiment. The other parameters were configured as follows: the maximum perception range of the laser scanner falls in [0.1m, 3m]; the look ahead distance is 0.4m; the translational speed is 0.3m/s; the maximum rotational speed is 1rad/s.

The robot paths in the simulation are recorded in Figure 8, where the black dots are the estimated robot positions, the magenta dots are the true robot positions and the red curve is the given path which starts from S_1. The four key uncertainty evaluators $\|\hat{\delta}_D\|$, $\hat{\delta}_\theta$, $E(\|\hat{\delta}_D\|)$ and $E_\theta(\hat{\delta}_\theta)$ were calculated for each position along the path and plotted as Figure 9, where the blue and black solid curves near the left vertical axis are the $\|\hat{\delta}_D\|$ and the $\hat{\delta}_\theta$ values, respectively, the red and magenta dashed curves near the right vertical axis, denoted as E_s, are the $E(\|\hat{\delta}_D\|)$ (simplified as E_D) and the $E_\theta(\hat{\delta}_\theta)$ (simplified as E_θ), respectively, and the horizontal axis is the k_p of the robot along the path. These curves and the horizontal axis have the same meanings in the following Figures 8.
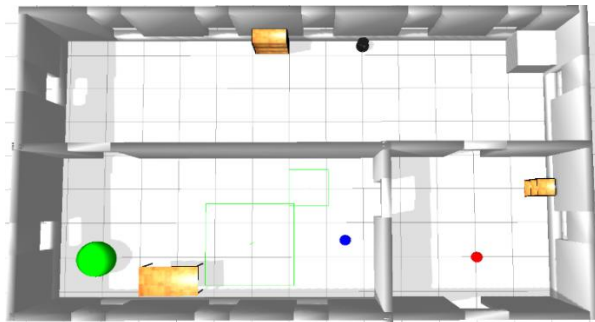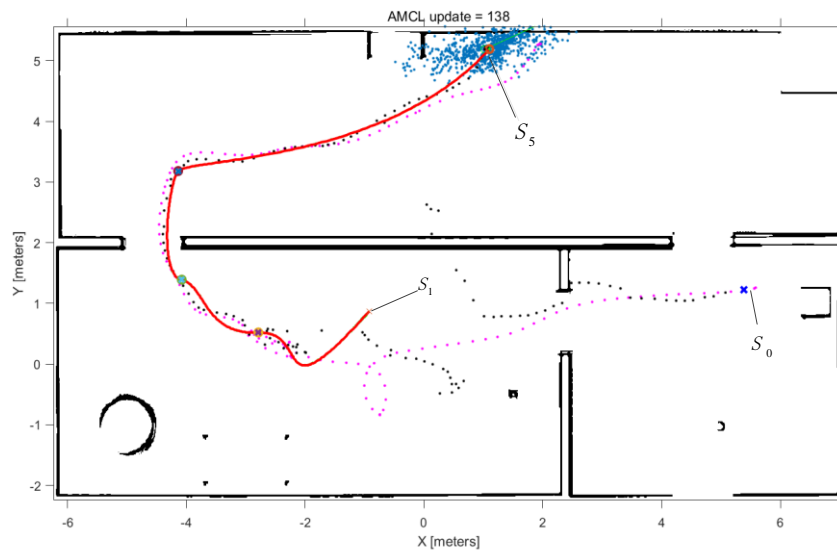

Figure 7. Simulation environment

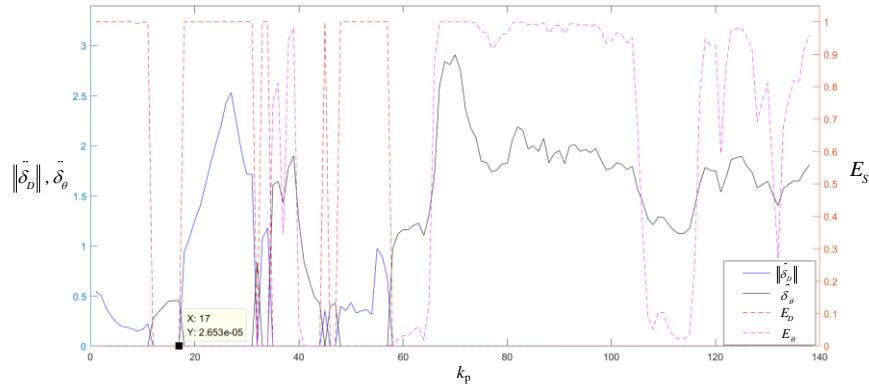*Figure 8. Simulated robot paths*

*Figure 9. The four key uncertainty evaluators along the path*

It can be seen from Figure 9 that, as the robot moved from the 18th position to the 60th position, the value of E_D mostly increased to 1 and that of $\|\hat{\delta}_D\|$ mostly surpassed 0.942m. This means the uncertainty in the estimation of X-Y coordinates is so large that the robot cannot follow the given path.

As shown in Figure 8, the robot deviated greatly from its true position before the 60th position, indicating that the robot motion is very unreasonable. In fact, before the 18th position, the value of E_D already reached 1 while that of $\|\hat{\delta}_D\|$ was less than 0.5m, which is unsafe for the robot. This is backed up by the corresponding section of the path in Figure 8: the localization results show that the robot went into a gate. Fortunately, the robot still moved across the gate despite the huge deviation between the estimated and true positions.

From the 60th positions onward, the robot's X-Y coordinates were estimated very accurately, which ensures the precision of the path following behavior. Figure 9 also shows that the value of E_θ was excessively large, which is proved by the corresponding path segment in Figure 8 that the robot failed to reach the destination.

5. Experimental verification

To further validate the proposed evaluation functions, the author conducted an experiment in an artificial environment (Figure 10 (a)). The experiment map and the 2 optimal paths are displayed in Figure 10(b). The map was drawn by simultaneous localization and mapping technology. In this experiment, a Pioneer 3-DX robot with a UTM-30LX laser scanner (Figure 11) was asked to follow the given path. The localization results were provided by the AMCL, while the maximum perception range of the robot was set to 2m. As in the previous simulation, the virtual vehicle path following algorithm was adopted at the translational speed of 0.2m/s and the rotational speed of 1 rad/s.
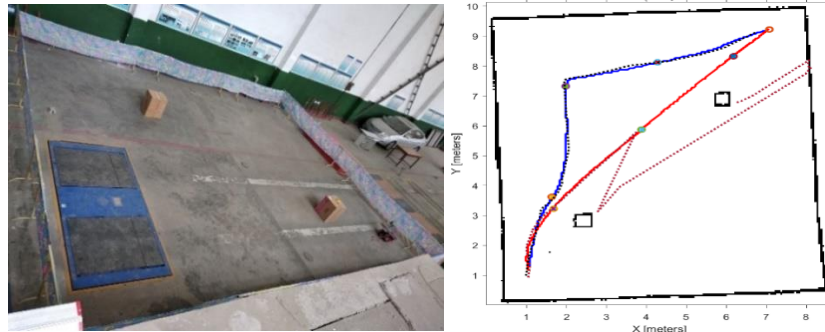
(a) Experiment environment (b) Experiment map, the optimal paths and the tracks

*Figure 10. Experiment environment and settings*

Figure 10(b) presents the two given paths in solid curves. Specifically, the blue curve is new optimal path determined by the proposed evaluation method considering localizability, while the red curve is the traditional optimal path obtained by the traditional method, which does not consider the localizability in path planning. The actual tracks of the robot in the experiment are also presented in Figure 10(b), with the black dotted curve being the track obtained by following the new optimal path and the brown dotted curve being the track acquired by following the traditional optimal path (Zhou and Lin, 2011).


Figure 11. The robot

As can be seen in Figures 10(a) and (b), the robot following the traditional optimal path lost its direction at about 78s into the experiment. By contrast, using the optimal path determined by our approach, the robot successfully arrived at the destination at 127s after the start of the experiment (Lankenau and Rofer, 2002). The same results

were observed from the evaluations of the uncertainty impact along the path. It can be seen from Figure 12(a) that the four key uncertainty evaluators were very small along the new optimal path, indicating that the uncertainty is so small that the robot can reach its destination safety. On the contrary, the results along the traditional optimal path in Figure 12(b) reveals that the AMCL outputted an excessively large $\|\hat{\delta}_D\|$ since the 75th position, resulting in a huge deviation from the given path in Figure 10(b). The values of the $\|\hat{\delta}_D\|$ and the E_D remained too high until the 115th position. As a result, the robot moved randomly and the localization results were totally wrong.
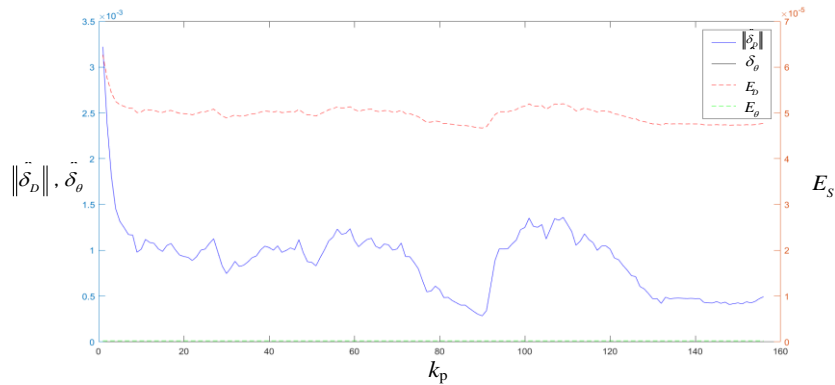
(a) Following the new optimal path
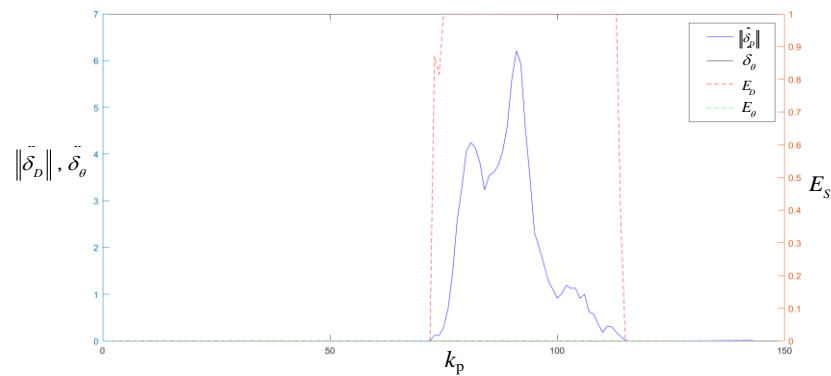
(b) Following the traditional optimal path

Figure 12. Evaluation of uncertainty impact

6. Conclusions

This paper mainly discusses the impact of localization uncertainty on path planning and path following. Assuming that the localization error reaches the covariance, the uncertainty of localization was safety represented by the half length of the possible distribution of X-Y coordinates and the variance of orientation,

separately. Then, the negative impacts of these factors on the path following of the robot were analyzed based on a simplified robot motion model. On this basis, two evaluation functions were developed to measure the uncertainty impacts. Simulation and experiment show that the evaluation functions successfully described the impacts of the uncertainty, and the function values are negatively correlated with the impact.

References

Censi A. (2007). On achievable accuracy for range-finder localization. in *Proceedings 2007 IEEE International Conference on Robotics and Automation*, pp. 4170-4175. https://doi.org/10.1109/ROBOT.2007.364120

Egerstedt M., Hu X., Stotsky A. (2001). Control of mobile platforms using a virtual vehicle approach. *IEEE Transactions on Automatic Control,* Vol. 46, No. 11, pp. 1777-1782. https://doi.org/10.1109/9.964690

Gonzalez J. P., Stentz A. (2007). Planning with uncertainty in position using high-resolution maps. in *Proceedings 2007 IEEE International Conference on Robotics and Automation*, pp. 1015-1022. http://dx.doi.org/10.1109/ROBOT.2007.363118

Hu C., Chen W., Wang J., Wang H. (2016). Optimal path planning for mobile manipulator based on manipulability and localizability. in *2016 IEEE International Conference on Real-time Computing and Robotics (RCAR),* pp. 638-643. https://doi.org/10.1109/RCAR.2016.7784104

Lankenau A., Rofer T. (2002). Mobile robot self-localization in large-scale environments. *IEEE International Conference on Robotics & Automation IEEE.* https://doi.org/10.1109/ROBOT.2002.1014732

Murtra A. C., Mirats-Tur J. M., Sanfeliu A. (2008). Action evaluation for mobile robot global localization in cooperative environments. *Robotics & Autonomous Systems,* Vol. 56, No. 10, pp. 807-818. https://doi.org/10.1016/j.robot.2008.06.009

Qian K., Ma X., Fang F., Dai X., Zhou B. (2016). Mobile robot self-localization in unstructured environments based on observation localizability estimation with low-cost laser range-finder and RGB-D sensors. *International Journal of Advanced Robotic Systems,* Vol. 13, No. 5, pp. 1-11. https://doi.org/10.1177/1729881416670902

Roy N., Burgard W., Fox D., Thrun S. (1999). Coastal navigation-mobile robot navigation with uncertainty in dynamic environments. in *Proceedings 1999 IEEE International Conference on Robotics and Automation (Cat. No.99CH36288C)*, Vol. 1, pp. 35-40. https://doi.org/10.1109/ROBOT.1999.769927

Wang Y., Chen W., Wang J., Wang H. (2015). Active global localization based on localizability for mobile robots. *Robotica,* Vol. 33, No. 8, pp. 1609-1627. https://doi.org/10.1017/s0263574714000940

Yang Z., Wu C., Zhou Z., Zhang X., Wang X., Liu Y. (2015). Mobility increases localizability: A survey on wireless indoor localization using inertial sensors. *ACM Comput. Surv.,* Vol. 47, No. 3, pp. 1-34. https://doi.org/10.1145/2676430

Zhao X. J., Li X., Tan T. (2000). A novel landmark tree based self-localization and path-planning method for an intelligent wheelchair. *IEEE International Workshop on Robot & Human Interactive Communication IEEE*. https://doi.org/10.1109/ROMAN.2000.892475

Zhou J. H., Lin H. Y. (2011). A self-localization and path planning technique for mobile robot navigation. *Intelligent   Control   &   Automation   IEEE*. https://doi.org/10.1109/WCICA.2011.5970604